Available online at www.sciencedirect.com
SCIENCE DIRECT®
Journal of Sound and Vibration 279 (2005) 119–139
JOURNAL OF SOUND AND VIBRATION
www.elsevier.com/locate/jsvi

Local damage detection using the two-dimensional gapped smoothing method

M.K. Yoon[a,*], D. Heider[a], J.W. Gillespie Jr.[b], C.P. Ratcliffe[c], R.M. Crane[d]

[a] *Center for Composite Materials, University of Delaware, Newark, DE 19716-3144, USA*
[b] *Department of Material Science & Engineering, Department of Civil & Environmental Engineering, Center for Composite Materials, University of Delaware, Newark, DE 19716, USA*
[c] *Mechanical Engineering Department, United States Naval Academy, Annapolis, MD 21402, USA*
[d] *Naval Surface Warfare Center, Carderock Division, Code 6553, West Bethesda, MD 20817-5700, USA*

Received 13 December 2001; accepted 28 October 2003

Abstract

This paper presents a procedure for locating variability in structural stiffness. For some types of structure, this variability is directly related to manufacturing defects and/or in-service damage. Unlike many published damage detection methods, the procedure presented here uses only data obtained from the damaged structure. Baseline data and theoretical models of the undamaged structure are not used during the analysis presented here. The procedure locates regions in a structure where the stiffness varies. Providing it is known that the structure, in its undamaged state, is homogeneous with respect to stiffness, the procedure will detect the areas of inhomogeneity that are caused by the incipient damage. For non-homogeneous structures, some knowledge of the structural details (for example, engineering drawings or a baseline test) is required in order to discriminate damage. The procedure is a two-dimensional generalization of a previously published one-dimensional gapped smoothing method, whereby local features in vibration curvature shapes are extracted using a localized curve fit (i.e., smoothing). A variability index is generated for each test point on the structure. Increased variability is due either to structural stiffness features or damage. A statistical treatment of the indices enables discrimination of areas with significant stiffness variability. Providing the damaged areas are sufficiently small compared to the total surface area, their indices will be statistical outliers. The procedure can either analyze mode shape data, or frequency dependent operating displacement shape data.

The procedure is demonstrated with a finite element model of a plate, and experiments on composite plates with deliberately induced multiple delaminations. Finally, the method is demonstrated on data taken from a large composite hull structure. In all cases the procedure successfully located the damaged regions.

*Corresponding author. Tel.: +1-302-831-2765; fax: +1-302-831-8525.
E-mail address: yoon@ccm.udel.edu (M.K. Yoon).

0022-460X/$ - see front matter
doi:10.1016/j.jsv.2003.10.058

1. Introduction

Structures with manufacturing defects and service damage show different dynamic responses from the equivalent structure without defects or damage. Vibration techniques offer the potential for locating both global and local defects in large-scale composite structures, for quality assurance/quality control (QA/QC) and non-destructive inspection (NDI).

Significant work has been done in localizing damage with vibration techniques [1]. Many of these techniques use modal parameters such as natural frequencies, damping factors, and mode shapes. Natural frequency information is used for the detection of damage [2] as well as characterization of debonding damage [3], delaminations [4], and elastic constant determination [5]. It may be difficult to use damping factors to detect damage because of significant measurement uncertainties, and localization is even more difficult [5,6]. Mode shape data has been used for local damage detection by many researchers [7–11]. However, these methods have difficulty in making the transition from research to practice because useful information on damage is lost during data processing (e.g., modal analysis) [12] or because linear models cannot clearly explain non-linear features such as crack opening and closing or crack propagation [13]. Non-linear system models are extensively studied to overcome the linear models. Depth of surface cracks in linear structures is estimated in terms of changes in frequencies and modes [14]. The curvature of the mode shape is increasingly used for the local damage detection because the curvature is proportional to the surface strain that is sensitive to the local changes in stiffness [7]. Pandey et al. [8] compared the curvatures of the mode shapes between the undamaged and damaged structures.

Other techniques use frequency response functions (FRF) [15,16] or operating deflection shapes [12] for local damage detection. System identification techniques [15] are used to obtain the eigenvalues and eigenvectors from the FRF, from which the mass and stiffness matrix are determined to correlate with the damage location. The operating curvature shapes have also been developed for local damage detections [12,16]. These non-resonant methods increase sensitivity for the location of damage when compared to methods based solely on resonant parameters (modal parameters). This is because non-resonant methods use information from all of the broadband frequencies, and also avoid the errors introduced during a modal analysis data reduction. In order to detect damage, Sampaio [16] directly subtracted the values of the operating curvature shape of the damaged structure from that of the undamaged structure.

Most of these techniques mentioned require either experimental baseline data or a mathematical model of the undamaged structure. As an example, Stubbs et al. [10] developed a damage localization method for a continuous beam, which does not require experimental baseline modal parameters. However, a finite element model was used to simulate the response of the undamaged structure to replace the baseline data from the undamaged structure. The parameters of the finite element model for the undamaged structure were obtained from the dynamic response of the damaged structure by employing a system identification method. Cornwell et al. [11] extended the one-dimensional strain energy method by Stubbs et al. [10] to two-dimensional structures, but their approach still requires baseline data from the undamaged structure.

Ratcliffe [7] developed the gapped smoothing method for the one-dimensional beam, which operates solely on data obtained from the damaged structure to locate structural stiffness variability. At first, only the resonant data such as mode shape data were used to detect the local

stiffness reduction in a notched steel beam [7]. Ratcliffe successfully used this approach to locate delamination in composite beams [9]. Later, broadband data were employed by using the frequency-dependent operating curvature shapes obtained from the FRF data. This approach significantly increased the sensitivity of the identification of structural variability [12]. Yoon et al. [17] developed the global smoothing method for the one-dimensional beam, which uses mode shape data and mathematical mode shape functions of the beams for the calculation of the structural irregularity index. This method showed improved performance over the gapped smoothing method by eliminating the smearing effect on the edges of the damage and the significant noise present in the original algorithm at the boundary edges of the structure. More recently, Yoon's method was refined to improve sensitivity (relative to approaches based on mode shape data) by superimposing the mathematical mode shape functions, enabling the use of frequency-dependent operating curvature shape data [18].

The present study extends the one-dimensional gapped smoothing method (1-D GSM) [7,12] to the two-dimensional gapped smoothing method (2-D GSM). In order to locate structural variability, these methods do not require baseline data from a presumably undamaged structure, since they predominantly identify regions of the structure where there is stiffness variability. When it is known that the structure is intended to be uniform and homogeneous, features located by the 1-D GSM and 2-D GSM can be attributed directly to damage or manufacturing defects. When it is possible to test a structure before and after some damage-causing incident, the damage can be identified by looking at the change in the structural irregularity indices developed by the procedures presented here. While this aspect of damage detection has proved to be most successful in the testing of large composite structures, this characteristic is not further addressed in this paper. The developed 2-D GSM method uses either broadband or resonant (modal) data obtained from any plate-like structure to generate structural irregularity indices. As described later, the irregularity is a stiffness variability. These irregularity indices are statistically treated to assess the damage potential with respect to a level of significance. The 2-D GSM is validated with finite element analysis (FEA) using mode shape data from a plate. It is experimentally verified with experiments on composite plates, in which both the mode shape and broadband methods are used. Finally, the results of a field test of a large composite hull structure are presented. The 2-D GSM successfully identified the size and locations of defects in all cases.

2. Theory

In this section, damage detection methods that use curvatures of both mode shape and broadband operating deflection shape data are presented to provide the theoretical background for the 2-D GSM.

2.1. Curvature subtraction method using mode shape data

Local stiffness changes in a beam result in a mode shape that has a local change in slope. Since the curvature mode shapes are related to the flexural stiffness of beam cross-sections [8], the change in curvature is used in this paper to locate local stiffness irregularity. If the structure is intended to be homogeneous, this stiffness irregularity relates directly to local damage or other

stiffness defect. The curvature (ϕ_i'') at the ith test grid point on the beam can be obtained to a Bachmann-Landau order of magnitude of $O(h^2)$ with the central difference approximation

$$\phi_i'' = (\phi_{i+1} + \phi_{i-1} - 2\phi_i)/h^2, \tag{1}$$

where ϕ_i is the mode shape obtained at the ith grid point and h is the uniform separation of the test grid. If damage is severe, there is a noticeable anomaly in the curvature of mode shapes at the location of damage. When the damage is less severe, further processing is needed to detect the curvature feature. Pandey et al. [8] directly obtained a damage index (δ_i) by calculating the absolute differences between the curvatures of the damaged and undamaged structures as

$$\delta_i = |\phi_{i,d}'' - \phi_{i,u}''|, \tag{2}$$

where $\phi_{i,d}''$ is the curvature at the ith grid point from the damaged structure, and $\phi_{i,u}''$ is the curvature from the undamaged structure. The damage index increases as the severity of damage increases.

2.2. *One-dimensional gapped smoothing method (1-D GSM) using mode shape data*

The 1-D GSM predominantly locates variations in structural stiffness. It uses mode shapes (8) obtained from the presumably damaged structure. These shapes are converted to curvature, and then processed to extract the anomaly in curvature coincident with the damage site. This processing is to fit a gapped cubic polynomial to the curvature mode shape. A structural irregularity index is then calculated as the difference between the measured shape and the calculated polynomial. Fig. 1 shows how to calculate the structural irregularity index using 1-D GSM. The continuous line represents the measured curvature mode shape, and the dotted line shows the cubic polynomial function at the ith grid point (C_i), which is defined as

$$C_i = a_0 + a_1 x_i + a_2 x_i^2 + a_3 x_i^3, \tag{3}$$

where x_i is distance between the ith grid point and the beam end. The coefficients a_0, a_1, a_2, and a_3 are determined explicitly using the neighboring curvatures from the damaged structure: ϕ_{i-2}'', ϕ_{i-1}'', ϕ_{i+1}'', and ϕ_{i+2}'' (the curvatures at the black marks as shown in Fig. 1). For the first and last two grid points the curvatures are calculated using four-point backward/forward looking finite

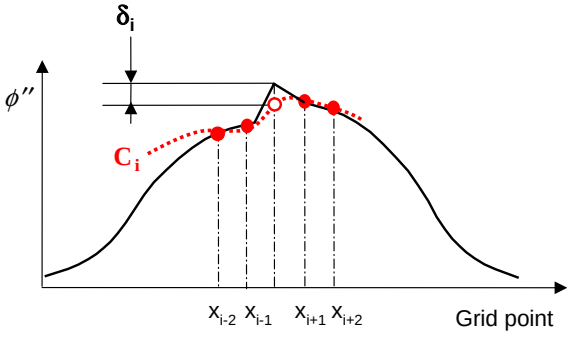

Fig. 1. Calculation of the structural irregularity index with the one-dimensional gapped smoothing method (the open circular mark shows the gapped point and the black circular marks show the used data points for the curvature curve smoothing).

difference approximation that maintain a Bachmann-Landau order of magnitude of $O(h^2)$ [11]. Then, the structural irregularity index is obtained as the squared difference between the cubic polynomial function and the curvature from the structure as

$$\delta_i = (\phi''_{i,d} - C_i)^2. \tag{4}$$

The structural irregularity indices are generally larger for parts of the structure with more stiffness variability (e.g., damaged locations or other localized structural stiffness features). However, there can be problems when damage exists at a node in the curvature mode shape. To overcome this problem the irregularity indices can be averaged for a number of analysis modes.

2.3. One-dimensional gapped smoothing method using operating deflection shape data

The 1-D GSM can also be used when the deflection shape is an operating deflection shape, rather than a mode shape [12]. The operating deflection shape is obtained by taking the complex values of the FRFs ($\psi(\omega)$) at the selected frequency. The algorithm has to be modified to accept complex data. This is achieved by applying the 1-D GSM separately to the real and imaginary parts of the operating displacement shape. That is, the real and imaginary parts of the displacement shape are separately converted to curvature shapes, and the gapped smoothing algorithm is applied separately to the real and imaginary curvature shapes. The structural irregularity indices are calculated from a modified Eq. (4):

$$\delta_i = (\psi''_{i,d} - C_i)^2_{REAL} + (\psi''_{i,d} - C_i)^2_{IMAGINARY}. \tag{5}$$

The above procedure can be applied to the operating deflection shape for a single frequency. However, it is better to apply the procedure to broadband FRF data, and frequency average the results, with the maximum number of operating deflection shapes (and thus, analysis frequencies) being limited to the number of spectral lines in each FRF. Operating deflection shapes and the resulting structural irregularity indices have a large dynamic range, and without correction this would cause index values obtained from data near resonance to dominate. This would result in a reduced effectiveness of the off-resonant data in the identification procedure. It has been noted by many authors that vibration shapes are insensitive to even quite large amounts of damage. Therefore the dynamic range problem is addressed by normalizing each operating deflection shape prior to its differentiation to curvature. The advantages of using broadband data include a significant increase in sensitivity when compared to modal methods, as well as the elimination of the need to extract modal parameters from the measured FRF data.

2.4. Two-dimensional gapped smoothing method (2-D GSM)

The two-dimensional gapped smoothing method defined in this paper uses a gapped surface-smoothing algorithm instead of the gapped line-smoothing algorithm in the 1-D GSM previously described. First, the deflection shape ($\Psi_{i,j}$) is normalized by its root mean square values as follows:

$$\psi_{i,j} = \Psi_{i,j} \sqrt{Nx \cdot Ny / \sum_{i=1}^{Nx} \sum_{j=1}^{Ny} |\Psi^2_{i,j}|}. \tag{6}$$

In this equation, Nx and Ny are the number of x- and y-directional grid points respectively, i and j are the location indicators for the x- and y-direction, and $\psi_{i,j}$ (complex number) is the normalized deflection shape at grid point (i,j). The curvature operating shape is calculated by the central difference approximation at grid point (i,j) as follows:

$$\nabla^2\psi_{i,j} = (\psi_{i+1,j} + \psi_{i-1,j} - 2\psi_{i,j})/h_x^2 + (\psi_{i,j+1} + \psi_{i,j-1} - 2\psi_{i,j})/h_y^2. \tag{7}$$

In this equation $\psi_{i,j}$ can be either a mode shape or an operating deflection shape, and h_x and h_y are the horizontal and vertical grid increments, respectively. For the grid points on the edges, forward or backward difference approximations are applied. To obtain a smoothed curvature shape, the curvature shape obtained by Eq. (7) is expressed as a mathematical form:

$$\nabla^2\psi_{i,j} = \mathbf{g}_{i,j}^{\mathrm{T}}\boldsymbol{\theta}_{i,j}, \tag{8}$$

where $\mathbf{g}_{i,j}$ is the base function vector, which depends on only the locations of the grid points and $\boldsymbol{\theta}_{i,j}$ is a parameter vector whose values are estimated later. The elements of the base function vector should be chosen such that the curvature shape represented by Eq. (8) shows a smooth surface. In this paper, the base function and parameter vectors are constructed as follows:

$$\mathbf{g}_{i,j}^{\mathrm{T}} = [1, x_i, y_j], \quad \boldsymbol{\theta}_{i,j}^{\mathrm{T}} = [a_0, a_1, a_2]. \tag{9}$$

Since the base function is known at any grid point and the curvature is calculated by Eq. (7), the parameters ($\boldsymbol{\theta}_{i,j}$) that are also complex numbers can be estimated by an identification method. A contour plot of an operating curvature shape is shown in Fig. 2. The intersections of the dotted lines show the grid test points. The open circular symbols show the gapped points in the curve

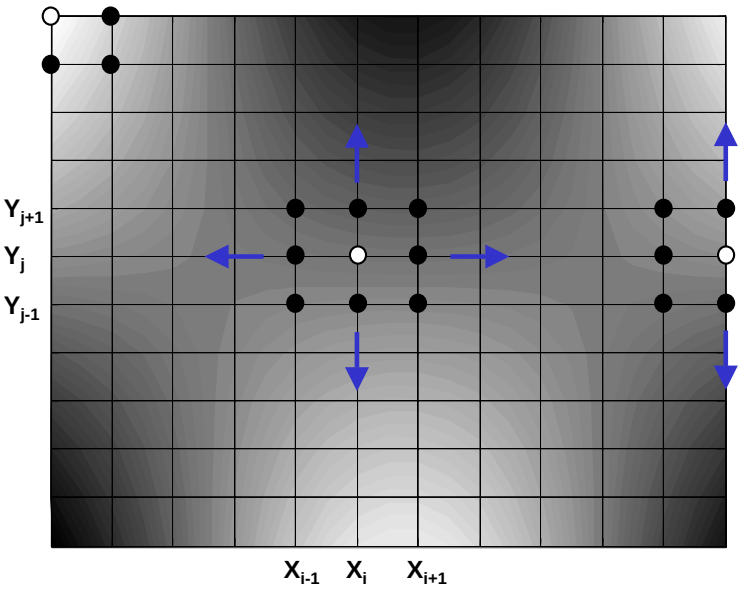

Fig. 2. Parameter estimation with the gapped neighboring data in a curvature shape for the two-dimensional gapped smoothing method (the open circular mark shows the gapped point and the black circular marks show the used data points for the curvature surface smoothing).

fitting, and the black circular marks represent the neighboring points to be used for the parameter estimation. Then, equation (8) can be arranged into a matrix form:

$$\boldsymbol{\lambda}_{i,j} = \mathbf{G}_{i,j}^{\mathrm{T}} \boldsymbol{\theta}_{i,j}, \tag{10}$$

where

$$\boldsymbol{\lambda}_{i,j}^{\mathrm{T}} = [\nabla^2\psi_{i-1,j-1}, \nabla^2\psi_{i,j-1}, \nabla^2\psi_{i+1,j-1}, \nabla^2\psi_{i-1,j}, \nabla^2\psi_{i+1,j}, \nabla^2\psi_{i-1,j+1}, \nabla^2\psi_{i,j+1}, \nabla^2\psi_{i+1,j+1}],$$

$$\mathbf{G}_{i,j}^{\mathrm{T}} = \{\mathbf{g}_{i-1,j-1}, \mathbf{g}_{i,j-1}, \mathbf{g}_{i+1,j-1}, \mathbf{g}_{i-1,j}, \mathbf{g}_{i+1,j}, \mathbf{g}_{i-1,j+1}, \mathbf{g}_{i,j+1}, \mathbf{g}_{i+1,j+1}\}$$

in the inner grid points. When the target point is on the edges or corners of the plate, the construction of the matrix $\mathbf{G}_{i,j}$ is slightly changed to match the neighboring grid points (see Fig. 2). Note that the number of the parameters should be the same or less than the number of neighboring points to enable explicit or least-squares estimation of the parameters:

$$\hat{\boldsymbol{\theta}}_{i,j} = (\mathbf{G}_{i,j}^{\mathrm{T}} \cdot \mathbf{G}_{i,j})^{-1} \mathbf{G}_{i,j}^{\mathrm{T}} \boldsymbol{\lambda}_{i,j}. \tag{11}$$

Then, the smoothed curvature shape is calculated by using the estimated parameters as follows:

$$C_{i,j} = \mathbf{g}_{i,j}^{\mathrm{T}} \hat{\boldsymbol{\theta}}_{i,j}. \tag{12}$$

Finally, the structural irregularity index is calculated:

$$\delta_{i,j} = |\nabla^2\psi_{i,j} - C_{i,j}|. \tag{13}$$

Note that the 2-D GSM is directly applied to complex $\psi_{i,j}$ in order to reduce noise in $\delta_{i,j}$ since the imaginary part has higher noise level by about an order of magnitude compared to the real part in $\psi_{i,j}$. Taking absolute values instead of squaring the difference improves the detection algorithm.

The structural irregularity indices can be summed over the obtained modes (when using mode shape data) or over the measured frequencies (when using operating curvature shape data). This procedure results in averaged indices ($\delta_{i,j}^{A}$):

$$\delta_{i,j}^{A} = \frac{1}{M} \sum_{\omega=\omega_i}^{\omega=\omega_f} \delta(\omega)_{i,j}, \tag{14}$$

where ω is the frequency (ω is the mode number in the case of the mode-averaged irregularity indices); ω_i and ω_f are the lowest and highest frequencies used in the averaging procedure, respectively; M is the number of spectral lines in the frequency range ω_i and ω_f (M is the number of experimentally available modes in the case of the mode-averaged method). This frequency averaging approach has been shown to increase the sensitivity of the damage detection method [12].

The averaged structural irregularity indices can further be treated statistically. The basic assumption is that the mean and standard deviation of averaged structural irregularity indices from the damaged structures in the undamaged area are similar to those from the repeated tests of an undamaged structure. Since these indices are averaged over frequency, the central limit theorem suggests that the set of averaged indices will be normally distributed. Thus, outliers from the normal distribution will be irregularity indices coincident with statistically significant features such as local damage or stiffness changes. Two outlier detection methods have been widely accepted over the years—Grubbs and Thompson's τ. The former is used where conservatism is

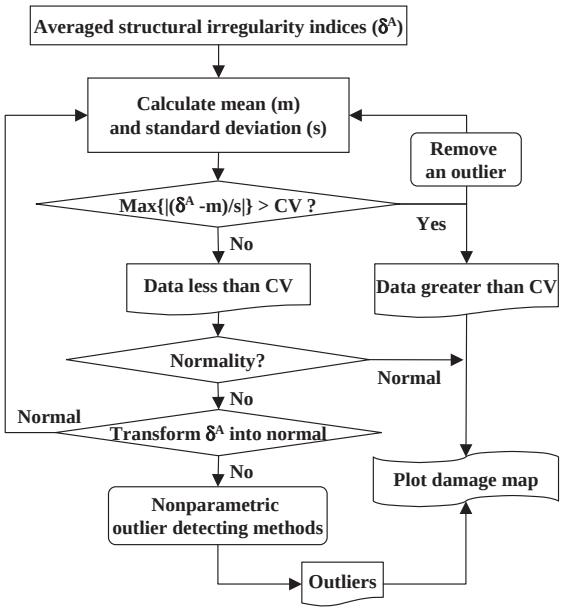

Fig. 3. Flow chart of statistical treatment for averaged structural irregularity indices ($\boldsymbol{\delta}^A$: averaged structural irregularity indices; CV: critical value).

important since it rejects fewer points than the latter. The present study adopted Grubbs' method that has been adopted by the ISO, ASME, and others [19].

Fig. 3 shows a procedure for the statistical treatment. First, if δ_k^A denotes the averaged structural irregularity indices at a grid point k, the maximum normed residual (MNR) is defined as

$$MNR = \max_k |(\delta_k^A - m)/s|, \tag{15}$$

where $k = 1, 2, \ldots, n$ and n is total number of grid points; m and s are the sample mean and standard deviation of the averaged structural irregularity indices, respectively. Next, MNR is compared to the critical value (CV) for the sample size n:

$$CV = \frac{t \cdot (n-1)}{\sqrt{n \cdot (n-2+t^2)}}, \tag{16}$$

where t is the $1 - \alpha/(2n)$ quantile of the Student-t-distribution with $n - 2$ degrees of freedom. The significance level of $\alpha = 1\%$ and/or 5% is used in the present study [20]. If MNR is larger than CV, the datum associated with MNR is declared to be an outlier; it is removed from the original data set and the procedure is repeated in the same way with the reduced data set until MNR becomes smaller than CV. Then, a hypothesis test (the goodness of fit to a normal distribution) is performed on the reduced data set. If the hypothesis of normality is accepted, the statistical treatment is finished. If the hypothesis is rejected, the data set can be transformed by some mathematical processes (for example, by taking logarithms), and the entire data rejection process

is repeated [21]. If normality is not obtained even after the transformation, non-parametric outlier detecting methods such as the Tchebychev inequality approach are used to detect the outliers [22].

All structural locations with an identified outlier are declared as "significant", and all other locations have their indices set to zero, yielding a final data set that consists of just the outliers from the statistical analysis. A structural irregularity contour map of this final data set can then be plotted.

3. Numerical examples

The 2-D GSM was applied to a $0.610\ \text{m} \times 0.305\ \text{m} \times 0.006\ \text{m}$ plate modelled using the commercial finite element code ANSYS, and the results are presented here. The domain was discretized with three-dimensional finite elements (Solid95, 20 nodes) of uniform size and the number of elements was $48 \times 24 \times 1$. The model had isotropic material properties and all-free-edge boundary conditions. Note that the present algorithm can be applied to any complex structure with any boundary conditions, and is not restricted to the demonstrative free boundary condition problem presented here. A damaged portion was modeled by reducing the modulus of the element by 30%. Figs. 4 (a)–(c) show Models I, II and III, respectively, with the damaged region (the reduced modulus area) shown on the plate model. The plate model had a total of 288 (24×12) grid points with a 0.025 m uniform step in both x- and y-direction. The first grid point was at the left lower corner (0.012 m, 0.012 m). There is no damage in Model I, and two types of damage (small and large) are designated in Models II and III. Model II has a small damage size of

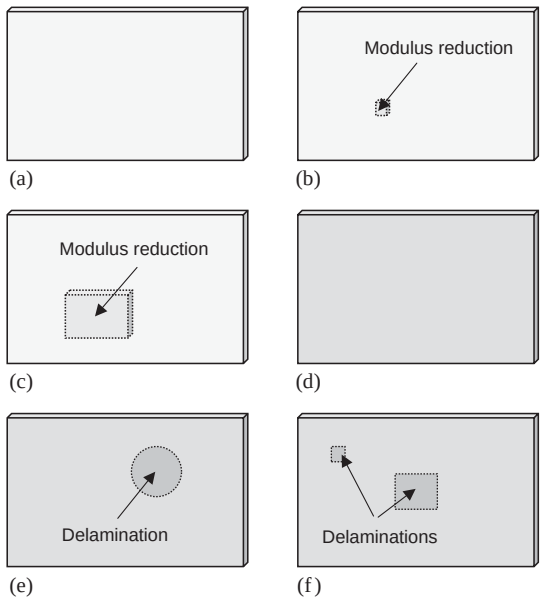

Fig. 4. Specification of the damage in the model plates. (a–c) show the FEA models with/without local modulus reductions; (d–f) show the experimental composite plates with/without delaminations). (a) Model I, (b) Model II, (c) Model III, (d) Model IV, (e) Model V, and (f) Model VI.

Table 1
Configuration of composite samples for the local damage detection

Model	Dimension (m) length × width × height	Damage type	Damage location: (x-GP, y-GP)	Damage size (m)	Used grid points
Model I	0.610 × 0.305 × 0.006	No damage	NA	0	24 × 12
Model II	0.610 × 0.305 × 0.006	Locally reduced stiffness	(10, 5)	0.025 × 0.025	24 × 12
Model III	0.610 × 0.305 × 0.006	Locally reduced stiffness	(11.5, 5.5)	0.15 × 0.10	24 × 12
Model IV	0.915 × 0.610 × 0.012	No damage	NA	0	18 × 12
Model V	0.915 × 0.610 × 0.012	Circular delamination	(11.5, 8)	0.127 diameter	18 × 12
Model VI	0.610 × 0.457 × 0.006	Two square delaminations	(6, 13.3) (12.2, 9)	0.025 × 0.025 0.087 × 0.075	24 × 18
Armor hull	(1.04 + 0.71) × 0.91 × (0.016/0.041)	Dry spot	(9.5, 5.5)	0.27 × 0.25	12 × 8

0.025 m × 0.025 m, which contains only one grid point. The large damage in Model III has a 0.152 m × 0.101 m size and spans 24 (6 × 4) grid points. The detailed specifications of Models I, II, and III are shown in Table 1, where the x-GP and y-GP represent x- and y-directional grid points, respectively. For example, x-GP 11.5 means that the damaged location was centered between grid points 11 and 12. The first six modes of vibration were extracted from the finite element modal analysis.

Fig. 5 shows the contour plots of the mode shapes for Model II. The mode shapes do not show any obvious features that can be associated with the damaged area. Fig. 6 shows the contour plots of the curvature mode shapes obtained by Eq. (7). The curvature shapes are shown in Fig. 6. This figure shows some features associated with the damaged area, but the features by themselves are not sufficiently significant to claim they have located the damaged region with any degree of confidence. The mode shapes for Models I and III are not shown in this paper, since there is minimal difference between the shapes for Model II and Models I and III. Similarly, the features in the curvature mode shapes for Model III are too small to identify the damage.

Fig. 7 shows the contour plots of the structural irregularity indices for the individual modes of Model II using mode shape data, where each mode shows a feature at the damage location. The figure shows that the flexural (beam-like) modes (1, 4, and 5) are better discriminators than the shear modes. Fig. 8 shows the contour plots of the structural irregularity indices for Model III with the large-size damage using the same method. It is worthy of note that when the damaged area is large, the 2-D GSM locates the edges of the damaged region. This is because the 2-D GSM uses a local smoothing method that uses only a small number of neighboring data points [9] around the gapped middle grid point in its surface fitting. Thus, for uniform damage, analysis that includes grid points only on a damaged region will find no structural irregularity, and the indices will be small. The 2D-GSM is, thus, an 'edge-finding' algorithm. The flexural modes (1, 4, and 5) also detect the edges of the damage area better than the shear modes (2, 3, and 6) in the case of Model III. These trends are consistent with the observations for Model II.

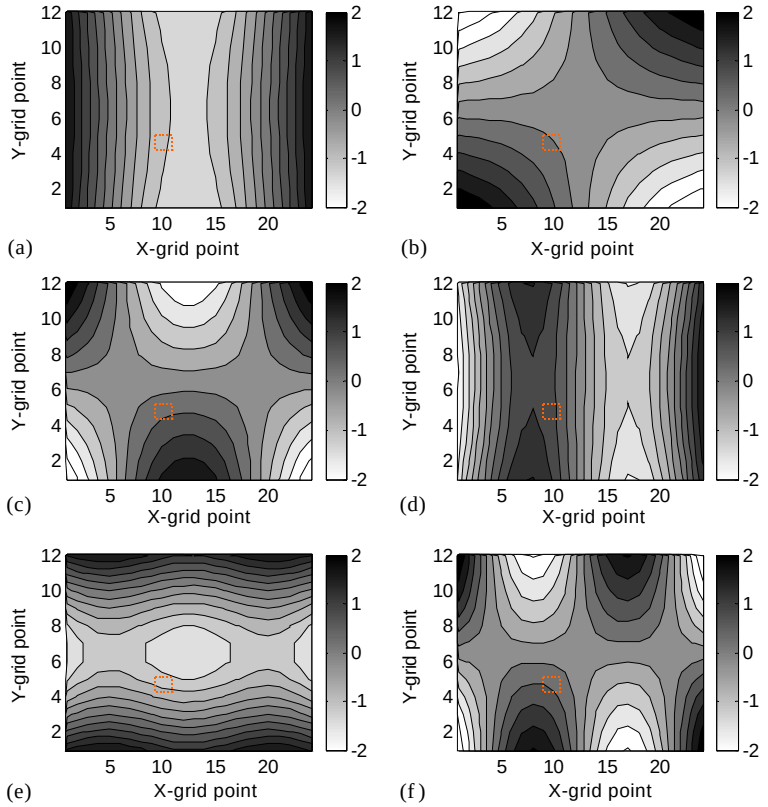

Fig. 5. Contour plot of the mode shapes for Model II (the dotted square shows the damaged region modeled by 30% modulus reduction). (a) Mode 1, (b) Mode 2, (c) Mode 3, (d) Mode 4, (e) Mode 5, and (f) Mode 6.

Figs. 9 (a)–(d) show the contour plots for Models II and III for both the mode-averaged and statistically treated structural irregularity indices. The mode-averaged index plots accurately define the location of the small-size damage, and the perimeter of the large-size damage. The statistical treatment successfully enhanced the plots, further improving the damage location capability.

Fig. 10 shows a histogram of the mode-averaged structural irregularity indices for three damage cases with the same geometry; no damage (Model I), small-size damage (Model II), and large-size damage (Model III). The outlier identification method correctly identified the irregularity indices for the damaged areas. Also correctly, it did not identify any of the indices from the undamaged model as outliers. Lilliefor's test [23] showed that, at the 5% level of significance, the mode-averaged irregularity indices after elimination of outliers are normal distribution, consistent with the earlier assumption. Table 2 compares statistics of the mode-averaged structural irregularity indices with and without outliers. As expected, eliminating the outliers reduces both the mean and standard deviation and reduces the differences in the mean and standard deviation between Models I, II, and III.

It is noted that as more modes are added to the averaging process, the sensitivity of the 2-D GSM increases, and uncertainty reduces. Hence, it is to be expected that better results may be

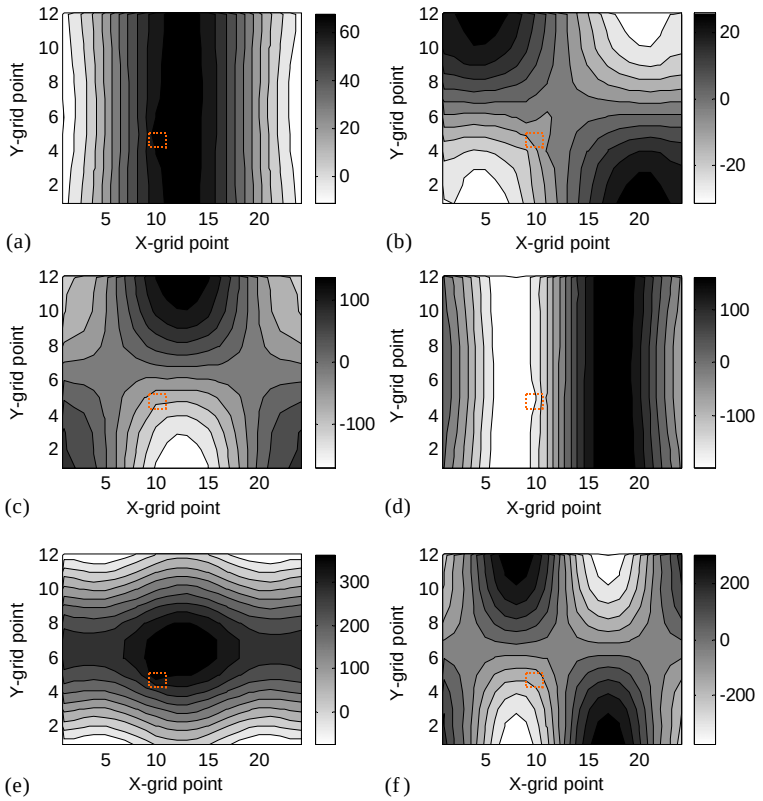

Fig. 6. Contour plot of the curvature mode shapes for Model II (the dotted square shows the damaged region modeled by 30% modulus reduction). (a) Mode 1, (b) Mode 2, (c) Mode 3, (d) Mode 4, (e) Mode 5, and (f) Mode 6.

expected as more modes are included in the summation. However, this FEA analysis did not include any errors associated with a mode-shape analysis of experimental data. Also, while a modal extraction from measured data will typically determine the major modes, real structures may have a very large number of lesser modes that may be omitted from the analysis. However, the effects of all of these modes are still included in the measured FRF data. This observation suggests that the broadband version of the 2-D GSM is preferred over the resonant (modal) version, since the problems associated with the modal extraction are entirely eliminated.

4. Experimental examples

4.1. Laboratory testing

The present method was applied to laboratory vibration tests of three composite plates, designated Models IV, V, and VI in Fig. 4 and defined in Table 1. Models IV and V were manufactured from woven E-Glass fabrics (24 oz/yd^2) and SC-15 Epoxy resins, and Model VI was manufactured from woven E-Glass fabrics (24 oz/yd^2) and Derakine 411-C-50 Vinyl ester

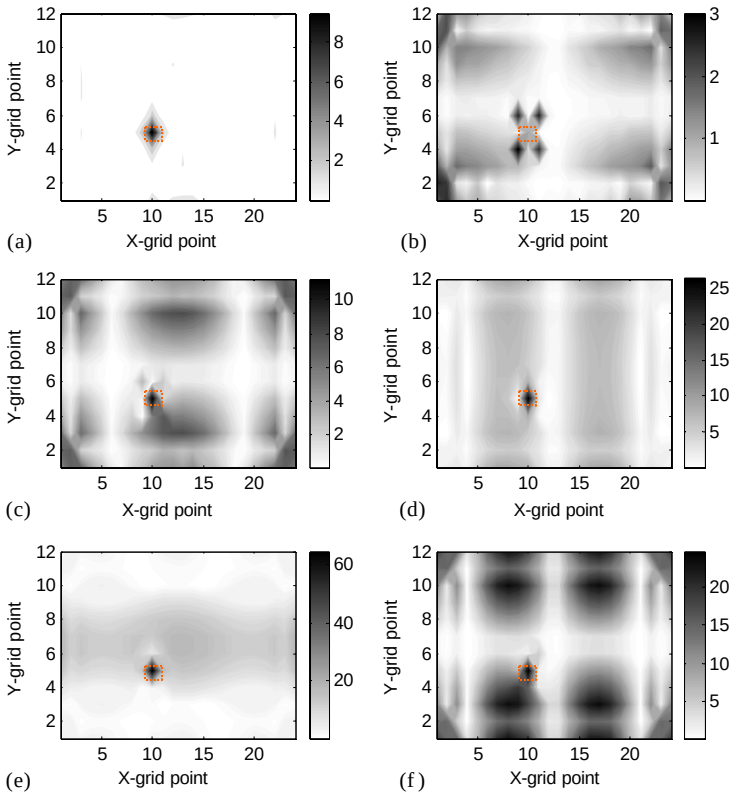

Fig. 7. Contour plot of the structural irregularity indices using mode shape data for Model II (the dotted square shows the damaged region modeled by 30% modulus reduction). (a) Mode 1, (b) Mode 2, (c) Mode 3, (d) Mode 4, (e) Mode 5, and (f) Mode 6.

resins. All the composite plates were made by the Vacuum Assisted Resin Transfer Molding (VARTM) process. A circular delamination (Model V) and two square delaminations (Model VI) were created by inserting Teflon films (0.0254 mm thick) at the mid-plane between layers. Model IV fabricated without any insert has the same geometry with Model V. The grid points were marked by a 0.051 m uniform step for the Models IV and V and 0.025 m uniform step for the Model VI, respectively, in both the x- and y-directions. The composite panels were suspended with two rubber bungee cords to approximate free-free boundary conditions. This boundary condition was chosen for simplicity and repeatability of experiments. The free boundary condition is not a prerequisite for the present method. A hammer with a force transducer was used to excite each grid point on the plate, and an accelerometer was used to measure acceleration at a corner of the plate. The acquired time domain signals were converted to the frequency domain by FFT, and the frequency averaged H1 frequency response functions between each grid point and the reference accelerometer were determined from three impacts at each test point.

During testing the data quality was predominantly monitored by the coherence functions. Fig. 11 shows the coherence functions averaged for all test points for Models IV and V. Overall, the data quality is excellent, with values typically greater than 99% (100% represents perfect,

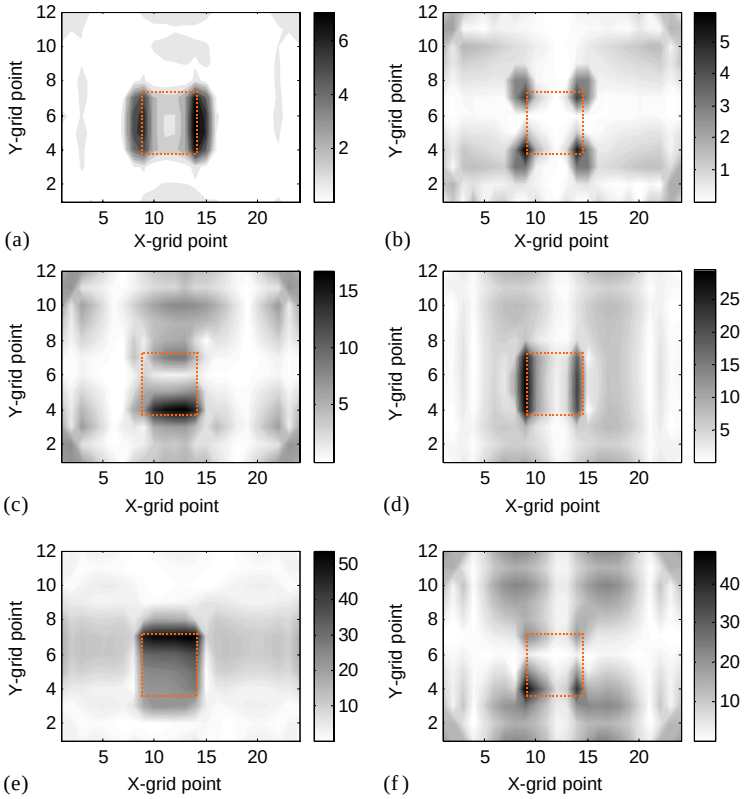

Fig. 8. Contour plot of the structural irregularity indices using mode shape data for Model III (the dotted square shows the damaged region modeled by 30% modulus reduction). (a) Mode 1, (b) Mode 2, (c) Mode 3, (d) Mode 4, (e) Mode 5, and (f) Mode 6.

noise free data). Based on this figure, the 2-D GSM method was applied to data from the frequency range 100 Hz to 2 kHz (ω_i and ω_f in Eq. (14)) for Models IV, V, and VI.

Figs. 12 (a)–(d) show the contour plots of the frequency-averaged and statistically treated structural irregularity indices for Models IV and V (without and with the circular delamination). The figure shows that the 2-D GSM successfully located the circular delamination, and the statistical treatment enhanced the result. As expected, the raw results for the plate without a deliberate delamination did not show any significant structural features. At the 5% level of significance the statistical treatment did not find any features on the plate without delaminations.

Fig. 13 shows histogram of the frequency-averaged irregularity indices for Model IV and V. The outlier identification method only detected the outliers in the damage region for Model V, and did not detect any outliers for Model IV. Lilliefor's test [23] showed that the hypothesis of normality was acceptable for all cases with significance level 1%. The statistics for Models IV and V are shown in Table 2.

Figs. 14 (a)–(d) show the contour plots of both the frequency- and mode-averaged structural irregularity indices with and without statistical treatment for Models VI that included two square delaminations of different sizes. The figure shows that both delaminations were detected using the

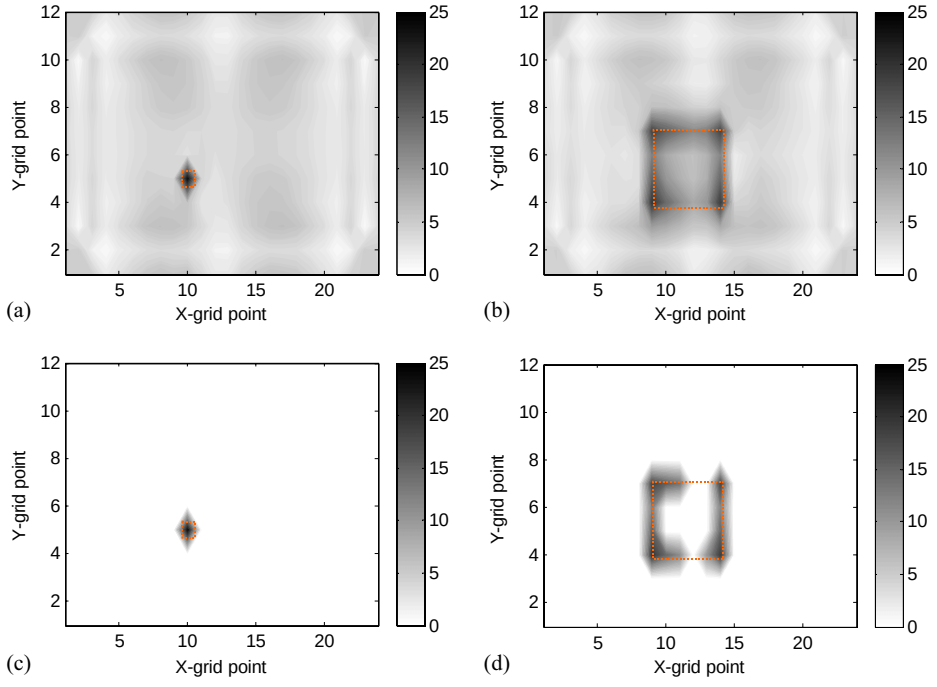

Fig. 9. Contour plot of the mode-averaged and statistically treated structural irregularity indices with 5% significance level (the dotted square shows the stiffness reduction region). (a) Mode-averaged structural irregularity indices for Model II, (b) mode-averaged structural irregularity indices for Model III, (c) statistically treated structural irregularity indices for Model II; and (d) statistically treated structural irregularity indices for Model III.

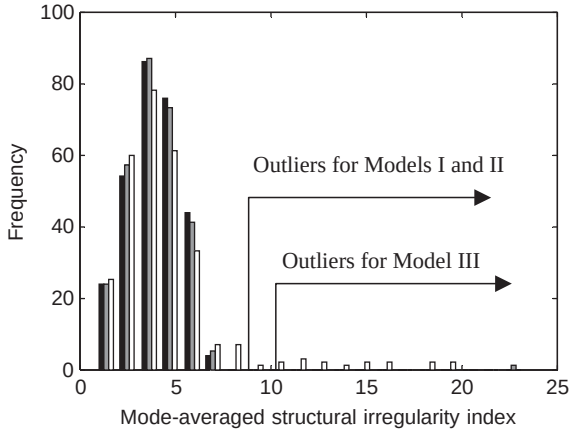

Fig. 10. Histogram and outliers of the mode-averaged structural irregularity indices with 5% significance level for Models I, II, and III: ▩, Model I; ▪, Model II; and □, Model III.

frequency-averaged version of the 2-D GSM, and the features on the plot were enhanced by the statistical treatment (at the 5% level of significance). Although not shown in the figures, reducing the level of significance to 1% enhanced the larger delamination feature, but suppressed the

Table 2
Statistics of the average structural irregularity indices with and without outliers

Data type	Model	Original data		Data without outliers	
		Mean	Std.	Mean	Std.
FEA	Model I	3.88	1.31	3.88	1.31
	Model II	4.03	1.71	3.88	1.30
	Model III	4.50	2.95	3.88	1.55
Experiments	Model IV	213.13	60.14	213.13	60.14
	Model V	231.42	83.86	225.68	68.20

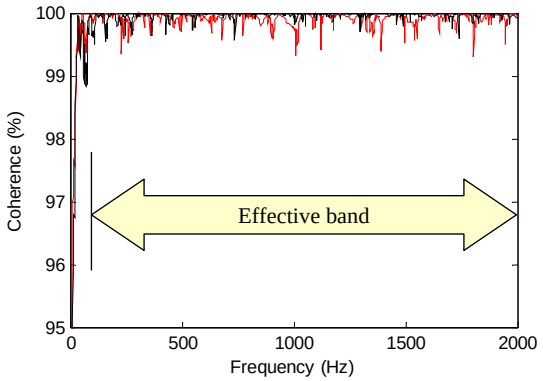

Fig. 11. Average coherence functions for Models IV and V: ——, Model IV; - - -, Model V.

smaller delamination. This shows the potential of the 2-D GSM to discriminate between areas with different levels of damage. The mode shape version of the 2-D GSM failed to detect the small-size delamination, even at the 30% level of significance. It is speculated that this may be because of the problems associated with the experimental modal parameter extraction. This result further confirms the previous observation that using the frequency-averaged operational deflection shape method offers less possibility of loosing essential information and gives increased sensitivity when compared to the modal method.

The results in Fig. 14 are based on the assumption that the averaged structural irregularity indices form normal distributions, but the normality test was rejected even with 1% significance level. When the Tchevychev inequality outlier detecting method [22] was applied to the averaged structural irregularity indices, both methods using ODS and mode shape data detected only the large-size delamination. Locating the small-size delamination was challenging for both methods. More refined grid spacing may increase sensitivity in detecting small-size damage. The relationship between grid spacing and defect size is a topic for further research.

4.2. *Large-scale composite structure testing*

The present method has also been applied to the large composite hull structure shown in Fig. 15. During VARTM processing, one area of the fabric was not properly infiltrated with resin

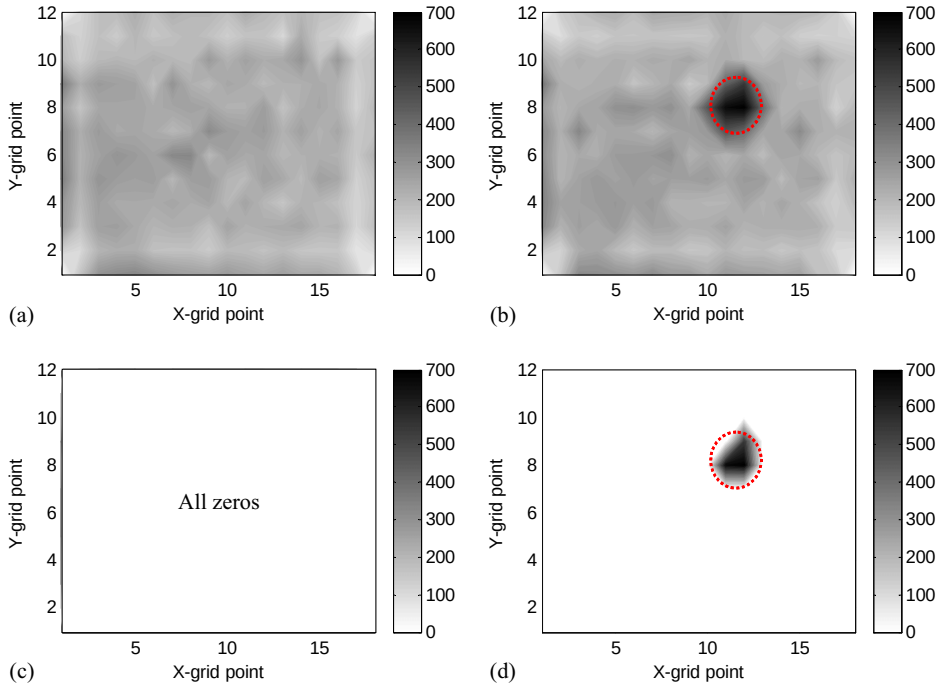

Fig. 12. Contour plot of the frequency-averaged and statistically treated structural irregularity indices with 5% significance level (the dotted circle shows the delamination region). (a) Frequency-averaged structural irregularity indices for Model IV; (b) frequency-averaged structural irregularity indices for Model V; (c) statistically treated structural irregularity indices for Model IV; and (d) statistically treated structural irregularity indices for Model V.

and a dry spot was formed. This dry spot consisted of only a few surface layers of the thick section, on the back surface, and it could not be seen from the front surface (see Fig. 16). Grid points were marked with a 0.075 m uniform increment in both x- and y-directions. For testing, the hull structure was suspended on rubber bungee cords. The primary reason for the test was to obtain a modal model, with the 2-D GSM analysis being secondary. Therefore, data were measured from more test points than were used for the 2-D GSM analysis. Fig. 17 shows the test mesh and one of the identified mode shapes. The area inside the dotted line shows the region that was used for the 2-D GSM analysis. Figs. 18 (a)–(d) compare the results from the 2-D GSM mode shape and operating deflection shape algorithms. In the figure the dotted square line highlights the physical location of the dry spot area. Both methods successfully detected the dry spot. However, the method using the operating deflection shape algorithm showed better discrimination, with less "noise" in the undamaged areas when compared to the method using the mode shape data. The results in Fig. 18 are based on the normality assumption, which was also rejected with 1% significance level. However, both the operating deflection shape and mode shape methods detected only the middle partial area of the dry spot when the Tchevychev inequality method was used. Note that the Tchevychev inequality method has tougher criterion in detecting outliers [19].

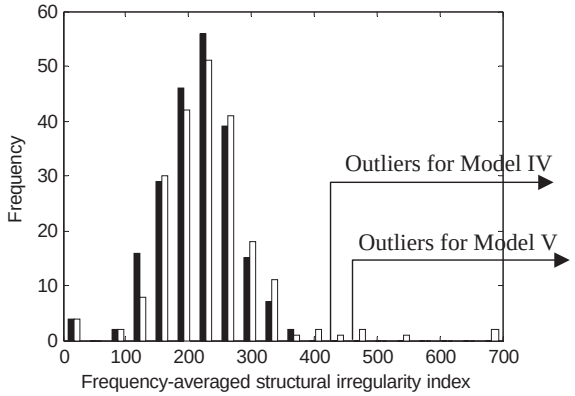

Fig. 13. Histogram and outliers with 5% significance level of the frequency-averaged structural irregularity indices for Models IV and V: ▩, Model IV; □, Model V.

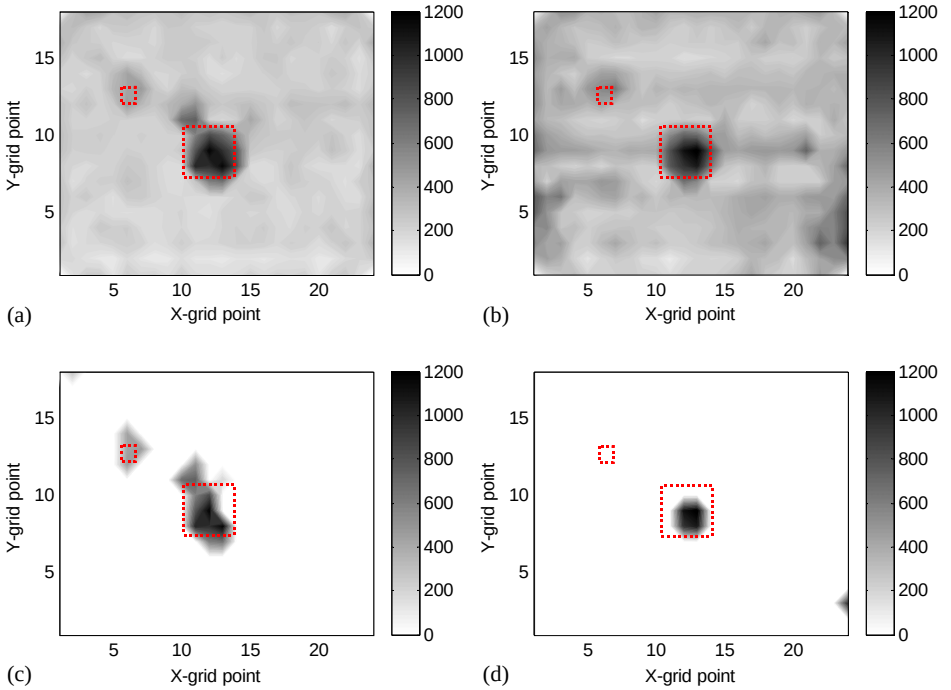

Fig. 14. Contour plots of the averaged and statistically treated structural irregularity indices with 5% significance level for Model VI (the dotted square shows the delamination region). (a) Frequency-averaged structural irregularity indices; (b) mode-averaged structural irregularity indices; (c) statistically treatment of the frequency-averaged structural irregularity indices; (d) statistically treatment of the mode-averaged structural irregularity indices.

5. Conclusions

In this paper, the one-dimensional gapped smooth method was successfully extended to two-dimensions, enabling regions of stiffness variability to be located in plate-like structural applications.

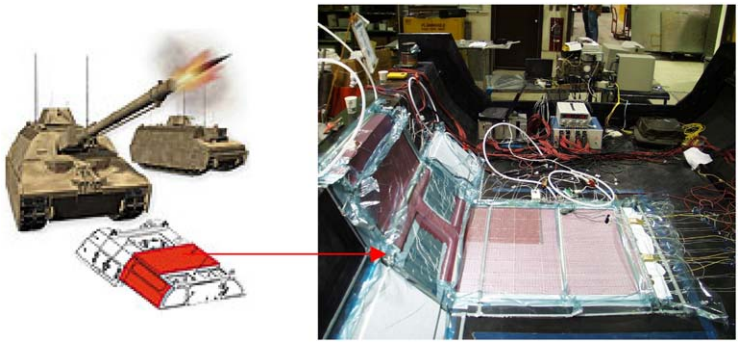

Fig. 15. VARTM manufacturing process of the composite hull structure.

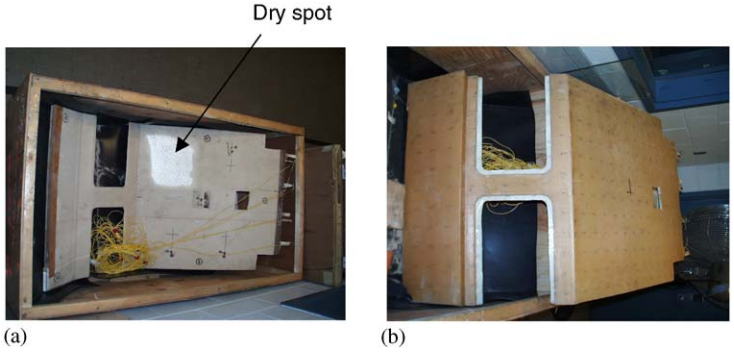

Fig. 16. Pictures of both surfaces of the composite armor hull structure. (a) Inside surface, and (b) outside surface.

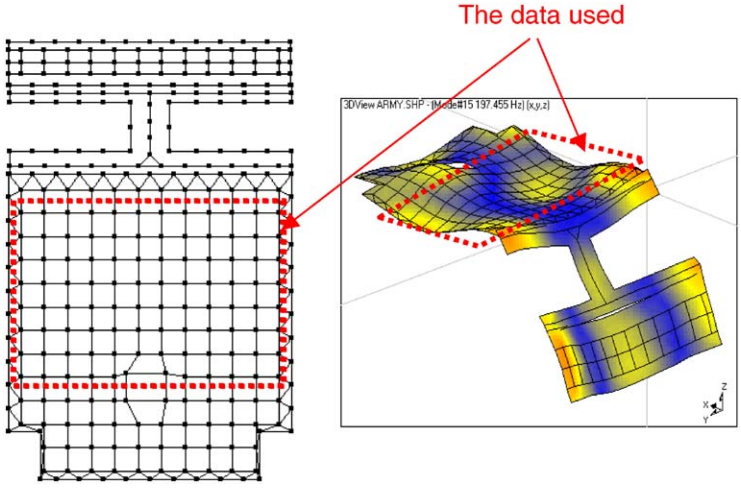

Fig. 17. Excitation grid points and an example of a mode shape for the composite armor hull structure (only the data obtained from the grid points in the dotted square are used in the damage detection algorithm).

A finite element model was used to assess the performance of the algorithm under idealized conditions. Experimental studies included composite plates having single and multiple delaminations of different sizes, and a composite hull structure that had a manufacturing defect on the surface.

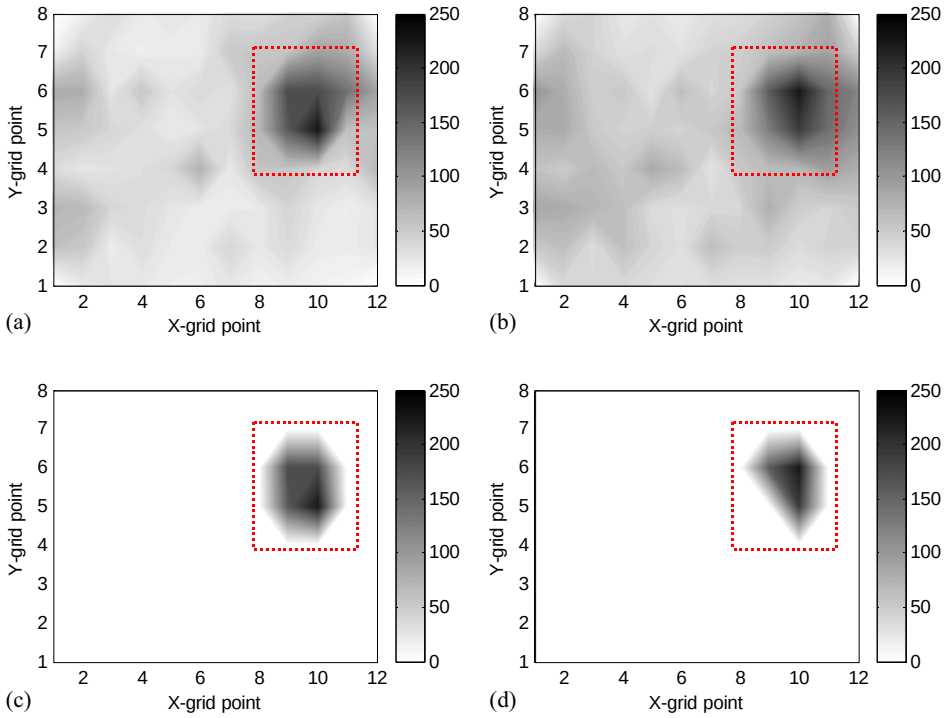

Fig. 18. Contour plots of the averaged and statistically treated structural irregularity indices with 5% significance level for the composite armor hull structure (the dotted square shows the dry spot area). (a) Frequency-averaged structural irregularity indices; (b) mode-averaged structural irregularity indices; (c) statistically treatment of the frequency-averaged structural irregularity indices; and (d) statistically treatment of the mode-averaged structural irregularity indices.

The present method detected the size and locations of small, localized stiffness reductions. When the structure (excluding the effects of damage) was globally homogeneous, and the damage area was small compared to the total testing area, the features located by the method were coincident with damage. This ability to locate the features was achieved without the need for either a mathematical model or a baseline test of the structure. This was possible because the underlying structure was homogenous and uniform with respect to stiffness, except for the areas of deliberately induced damage. In the case of large areas of uniform damage (compared to spacing and number of inspection points), however, the present algorithm identified the edges of the damage, which could make interpretation of the results more difficult. The results using the broadband operating deflection shape data showed superior performances over those using the resonant data (mode shapes) because the former method has more data points to average and less possibility to lose information in a modal parameter extraction. The structural irregularity indices were summed with respect to frequency or mode in order to increase sensitivity. The statistical treatment developed in the paper enhanced the ability to locate regions with stiffness variability.

The presented algorithm has direct applications for quality assurance/quality control and NDI of composite structures. Further studies are required to establish a quantitative relationship between the local stiffness reduction and the irregularity indices.

References

[1] Y. Zou, L. Tong, G.P. Steven, Vibration-based model-dependent damage (delamination) identification and health monitoring for composite structures—a review, *Journal of Sound and Vibration* 230 (2) (2000) 357–378.

[2] L.B. Crema, A. Castellani, G. Coppotelli, Damage localization in composite material structures by using eigenvalue measurements, *Materials and Design Technology* ASME PD-71 (1995) 201–205.

[3] A. Paolozzi, I. Peroni, Detection of debonding damage in a composite plate through natural frequency variations, *Journal of Reinforced Plastics and Composites* 9 (1990) 369–389.

[4] J.J. Tracy, G.C. Pardoen, Effect of delamination on the natural frequencies of composite laminates, *Journal of Composite Materials* 23 (1989) 1200–1215.

[5] R.F. Gibson, Modal vibration response measurements for characterization of composite materials and structures, *Composite Science and Technology* 60 (15) (2000) 2769–2780.

[6] R.M. Crane, Vibration damping response of composite materials, CCM Report 91-19, Center for Composite Materials, University of Delaware, Newark, DE, 1991, p. 277.

[7] C.P. Ratcliffe, Damage detection using a modified Laplacian operator on mode shape data, *Journal of Sound and Vibration* 204 (3) (1997) 505–517.

[8] A.K. Pandey, M. Biswas, M.M. Samman, Damage detection from changes in curvature mode shapes, *Journal of Sound and Vibration* 145 (2) (1991) 321–332.

[9] C.P. Ratcliffe, W.J. Bagaria, Vibration technique for locating delamination in a composite beam, *American Institute of Aeronautics and Astronautics Journal* 36 (6) (1998) 1074–1077.

[10] N. Stubbs, J.-T. Kim, Damage localization in structures without baseline modal parameters, *American Institute of Aeronautics and Astronautics Journal* 34 (8) (1996) 1644–1649.

[11] P. Cornwell, S.W. Doebling, C.R. Farrar, Application of the strain energy damage detection method to plate like structures, *Journal of Sound and Vibration* 224 (2) (1999) 359–374.

[12] C.P. Ratcliffe, A frequency and curvature based experimental method for locating damage in structures, *Transactions of the American Society of Mechanical Engineers Journal of Vibration and Acoustics* 122 (2000) 324–329.

[13] T.G. Chondros, A.D. Dimarogonas, Influence of cracks on the dynamic characteristics of structures, *Journal of Vibration, Acoustics, Stress and Reliability in Design* 111 (1989) 251–256.

[14] A.D. Dimarogonas, Vibration of cracked structures-a state of the art review, *Engineering Fracture Mechanics* 5 (1996) 831–857.

[15] W.H. Tsai, J.C.S. Yang, Nondestructive evaluation of composite structures using system identification technique, *Transactions of the American Society of Mechanical Engineers Journal of Engineering Materials and Technology* 110 (1988) 134–139.

[16] R.P.C. Sampaio, N.M.M. Maia, J.M.M. Silva, Damage detection using the frequency-response-function curvature method, *Journal of Sound and Vibration* 226 (5) (1999) 1029–1042.

[17] M.K. Yoon, D. Heider, J.W. Gillespie Jr., C.P. Ratcliffe, R.M. Crane, Local damage detection using a global fitting method on mode shape data, *IMAC XIX*: *A Conference on Structural Dynamics*, Vol. 1, Kissimmee, FL, February 5–8, 2001, pp. 231–237.

[18] M.K. Yoon, D. Heider, J.W. Gillespie Jr., C.P. Ratcliffe, R.M. Crane, Spatial damage detection in composite structures using a global fitting method on curvature operating shapes, *American Society for Composites 16th Annual Technical Conference*, Virginia Tech, Blacksburg, VA, September 9–12, 2001, WA-2, 100.

[19] R.B. Abernethy, B. Ringhiser, The history and statistical development of the new ASME-SAE-AIAAISO measurement and uncertainty methodology, *20th AIAA/SAE/ASME Joint Propulsion Conference*, AIAA-85-1403, New York, NY, July 1985, pp. 1–9.

[20] D. Neal, M. Vangel, Statistical analysis of mechanical properties, in: C.A. Dostal (Ed.), *Engineered Materials Handbook*, Vol. 1: Composites, American Society of Metals Press, Metals Parks, OH, 1987, pp. 302–307.

[21] B. Iglewicz, D.C. Hoaglin, *How to Detect and Handle Outliers*, American Society for Quality, Quality Press, Milwaukee, 1993, p. 87.

[22] L.D. Chen, *Lecture Notes*: *Experimental Engineering*, Department of Mechanical Engineering, The University of Iowa, Iowa City, IOWA, 1996, p. 75.

[23] *Statistics Toolbox*, The MathWorks, Inc., Natick, MA, 1993.